A Visible-Opaque Infrared-Modulator Fabric for Human Body Thermoregulation at Low Temperatures

Mohamed Boutghatin, Claire Pirim, Valérie Gaucher, Yannick Coffinier, Bahram Djafari-Rouhani, Vincent Thomy, Yan Pennec, Michèle Carette

ACS OMEGA

Open Access

http://pubs.acs.org/journal/acsodf

Article

A Visible-Opaque Infrared-Modulator Fabric for Human Body Thermoregulation at Low Temperatures

Mohamed Boutghatin,* Claire Pirim, Valérie Gaucher, Yannick Coffinier, Bahram Djafari Rouhani, Vincent Thomy, Yan Pennec, and Michele Carette

Cite This: *ACS Omega* 2026, 11, 9826−9835

Read Online

ACCESS | Metrics & More | Article Recommendations | Supporting Information

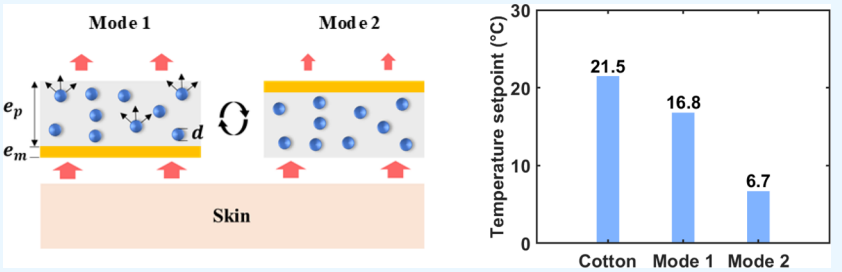

ABSTRACT: Optimizing textiles for enhanced passive radiative thermoregulation properties represents a significant step forward in technological innovation. To achieve this goal, we fabricated and characterized a visible-opaque infrared-modulator fabric (VOIMF) that can provide the human body with continuous thermoregulation at low temperatures. The fabric is a bilayer emitter composed of a polyethylene (PE) membrane and an ultrathin gold (Au) layer. The PE membrane contains randomly dispersed titanium dioxide (TiO_2) microparticles (MPs). By flipping the fabric, we demonstrate that the VOIMF can modulate the emissivity toward the environment in the mid-infrared range, thereby providing a thermal comfort zone over a large temperature range of ∼ 10 °C (from 6.7 to 16.8 °C). Moreover, the VOIMF is opaque in the visible (VIS) range and exhibits a white appearance, similar to cotton, due to the high light scattering property of TiO_2 MPs.

1. INTRODUCTION

Wearable textiles are essential to our daily lives, providing not only opacity in the visible range but also thermal comfort by adjusting the local temperature around our body. While technical textiles for outdoor use offer relatively sophisticated thermal comfort solutions (commercial textile references such as Omni Heat),[1] the situation for indoor spaces remains a vast area of study. Thus, the sensation of thermal discomfort experienced by an individual at rest in a closed room prompts them either to adjust the temperature of the room as a whole (by modifying the heating or air conditioning) or to add or remove layers of clothing textile to keep their body in thermal comfort. Conventional textiles used for clothing can therefore reduce the energy used to regulate our body temperature and are then part of the solution to limiting greenhouse gas emissions. Optimizing their thermal properties represents a promising approach to reducing our environmental impact while improving our thermal comfort.

The number of papers setting out strategies for improving the thermoregulatory performance of textiles has been growing steadily over the past decade, demonstrating the importance of this issue. The human body at 34 °C emits electromagnetic waves in the mid-infrared (MIR) range which are responsible for more than 50% of heat loss.[2] This high contribution has motivated researchers to design several radiative textiles for heating and cooling functionality based on the modulation of MIR radiations.[3−20] Very recent reviews on the subject present a highly exhaustive state of the art.[21,22] However, many radiative textiles can provide thermal comfort only over a narrow ambient temperature range, which limits their thermoregulation performances in terms of scope of application. Consequently, designing a textile that can ensure thermal comfort of the human body in a wide range of indoor temperatures remains a great challenge. To achieve this goal, various designs have been proposed, including fiber and membrane structures. These studies demonstrated dual-mode textiles composed of a multilayer with low and high emissivity faces, capable of switching between heating and cooling functions.[23−27] A dynamic structure has also been proposed to maintain the state of comfort.[28−32] However, the majority of these systems require external energy input, and the realization

Received: October 7, 2025
Revised: January 20, 2026
Accepted: January 22, 2026
Published: February 1, 2026

of such textiles remains challenging, particularly on a large scale.

Here, we proposed to study a visible-opaque infrared-modulator fabric (VOIMF) with high thermoregulating performances and opacity in the visible wavelength range. The VOIMF consists of a bilayer structure made up of a thin polymer film containing dielectric microparticles (MPs), covered by an ultrathin metallic film. The behavior of this asymmetric membrane with respect to the electromagnetic wave in both the VIS and MIR wavelength ranges is theoretically reported and experimentally demonstrated with the help of a commercial doped polyethylene (PE) membrane. Based on a systematic theoretical modeling of the geometrical and physical parameters of the membrane, we show that the structure exhibits asymmetrical MIR properties for the two modes used. Therefore, switching between the two modes is achieved by simply turning the fabric inside out. Moreover, VOIMF takes advantage of the collective scattering property of MPs to achieve high opacity in the VIS range.

2. RESULTS AND DISCUSSION

2.1. Fabric Design

2.1.1. Geometry and Working Principle. The proposed design consists of a polymer membrane of thickness e_p covered with an ultrathin metallic layer of thickness e_m. The polymer membrane is doped with dielectric particles randomly and uniformly dispersed in the polymer matrix (Figure 1). The

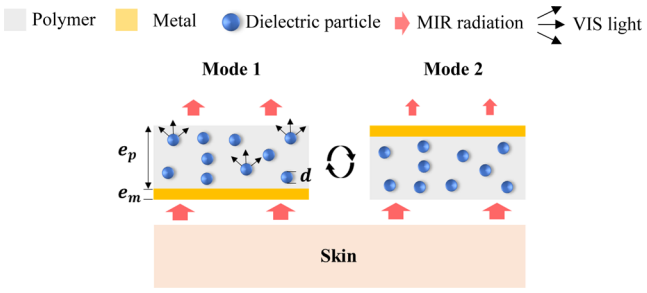

Figure 1. 2D schematic diagram illustrating the working principle of the VOIMF. When the high-emissivity layer (polymer with particles) faces outward, the fabric operates in Mode 1, resulting in a significant heat transfer to the environment. When the fabric is turned inside out (with the metal facing outward), the emissivity decreases and the fabric operates in mode 2.

operating mechanism of the VOIMF design is illustrated in Figure 1. When the PE composite membrane is exposed to ambient air, the external MIR emissivity is high due to the particle absorption, and the fabric acts as an infrared transmitter (Mode 1). On the contrary, low external emissivity is achieved when the metal layer faces the environment. In this case, the external MIR emissivity is low due to the high reflectivity of metal, and the fabric behaves as an infrared reflector (Mode 2). By turning the fabric inside out, the MIR emissivity of the outer face is then adjusted, allowing the fabric to be switched from Mode 1 to Mode 2.

2.1.2. Materials. We first discuss the optical and thermal properties of the different constituents that compose the fabric. PE is a polymer with high transparency in the MIR and VIS wavelength ranges[33] principally due, in the 5−15 μm range, to a limited number of vibrational modes.[34] It shows only narrow absorption peaks around the wavelengths of 6.8, 7.3, and 13.7 μm.[35] In addition, PE is a well-known polymer commonly used in energy and sustainable development applications.[34,36] Adding multiple layers may compromise the flexibility of the textile. To overcome this limitation, we propose incorporating absorbing particles directly into the polymer membrane, as a replacement for the additional absorbing layers used in previous studies.[23−27] Titanium dioxide (TiO_2) particles exhibit not only high absorption (emissivity) in the MIR range but also significant scattering in the VIS range due to their high refractive index.[37,38] The high absorption of TiO_2 in the 13−15 μm range is related to the Ti−O−Ti stretching vibration.[39] Although this goes beyond the fundamental work presented in this paper on the optical and thermal characterization of an asymmetrical sample of a polymer membrane loaded with particles and metallized, it should be noted that, in addition to these properties, TiO_2 has interesting characteristics for textile applications: it has been demonstrated that the incorporation of TiO_2 nanoparticles into textiles imparts antibacterial activity, adequate UV protection, and good crease resistance, thereby enhancing both performance and durability.[40] Other particles such as silicon oxide (SiO_2) and Carbone can also be used to enhance the absorption of PE, owing to the significant imaginary part of their refractive index in the 5−15 μm range. However, TiO_2 represents an excellent choice due to its dual effect in both the visible and infrared ranges: its strong scattering efficiency in the visible enhances optical opacity and promotes a cotton-like appearance, while its infrared properties contribute to improving the thermoregulation performance of the textile. The metal layer acts as a perfect mirror in the MIR range and therefore fully reflects infrared radiations while presenting a high thermal conductivity. While gold (Au) was selected due to its biocompatibility, it may be replaced by lower-cost metals with high MIR reflectance (e.g., silver or copper) that exhibit a similar refractive index over the 5−15 μm range. Even if we use standard PE in our work, to ensure good breathability of the metallized membrane, the metallic layer can also be deposited on nanoporous PE, which exhibits MIR optical properties similar to those of the standard PE, as demonstrated in[1]. Furthermore, adding a protective polymer membrane with low infrared absorption can significantly improve the durability of the VOIMF and ensure the maintain of its thermoregulation performance after washing.[1] For improved membrane flexibility, the continuous metallic layer can also be replaced by a discontinuous metallic layer while preserving the desired functionalities.[28]

2.2. Modeling

We propose here a systematic theoretical study of the optical properties of the fabric, and more specifically that of the PE composite membrane, as a function of the diameter (d) and volume fraction (f) of the particles and the thickness of the membrane (e_p). The optical properties were calculated using the Finite Element Method (FEM)-based modeling in COMSOL Multiphysics (see the Methods section), along with the transfer matrix method (TMM),[41] Mie theory,[42] and the effective medium theory (EMT).[43]

2.2.1. Particle Size Effect. The effect of particle size on MIR properties has been demonstrated by calculating both the extinction $\Sigma_e = \frac{4\sigma_e}{\pi d^2}$ and scattering $\Sigma_s = \frac{4\sigma_s}{\pi d^2}$ normalized cross sections of a single TiO_2 particle embedded in a PE medium. We can then deduce the absorption cross section using the relationship $\Sigma_a = \Sigma_e - \Sigma_s$. The calculations were performed by

https://doi.org/10.1021/acsomega.5c10457
ACS Omega 2026, 11, 9826−9835

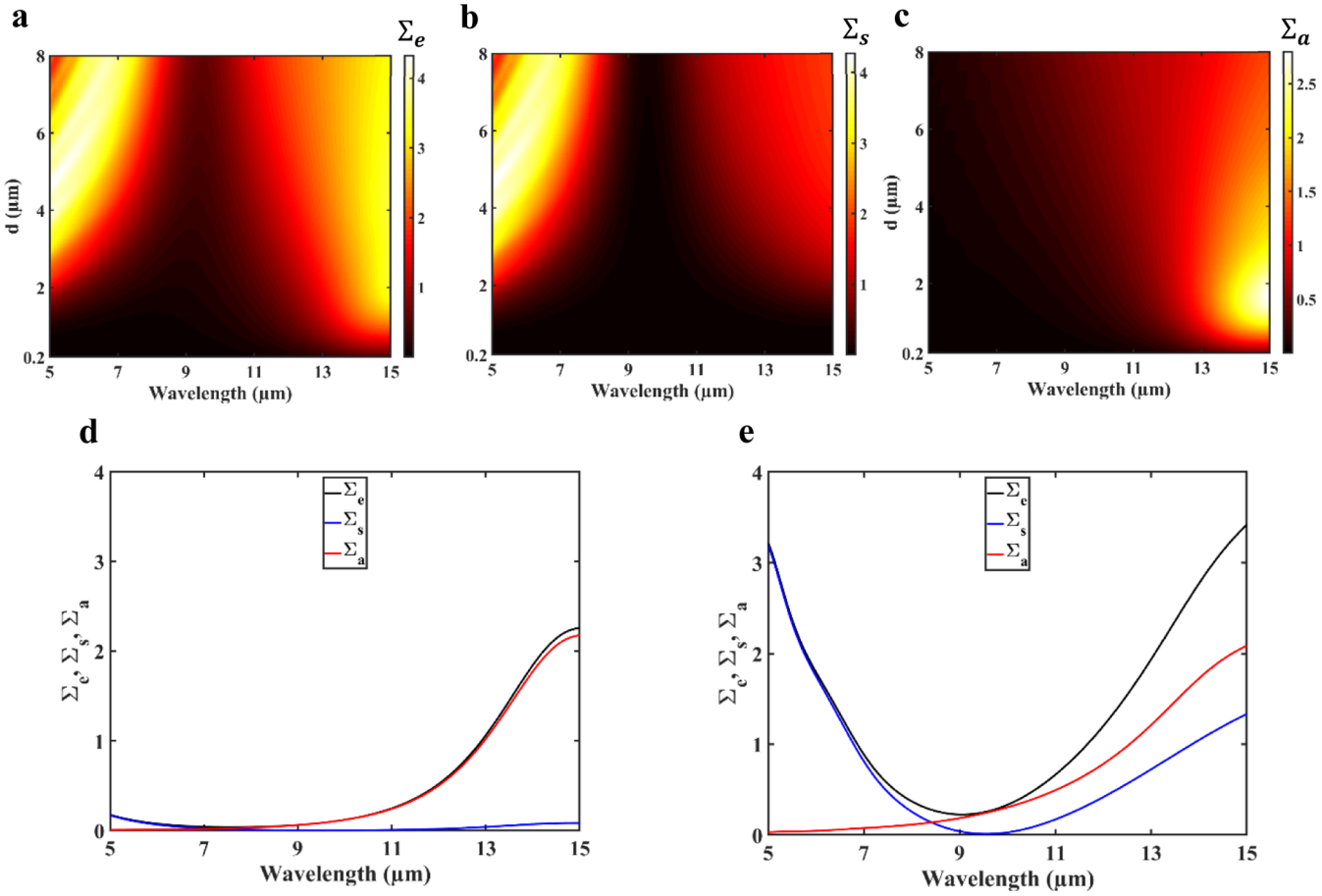

Figure 2. Normalized cross section of extinction Σ_e (a), scattering Σ_s (b), and absorption Σ_a (c) as a function of particle diameter d in the MIR range of 5−15 μm. Σ_e (black line), Σ_s (blue line), and Σ_a (red line) for d = 1 μm (d) and d = 3 μm (e). The calculation was done for a single TiO_2 particle in the PE medium by using Mie theory.

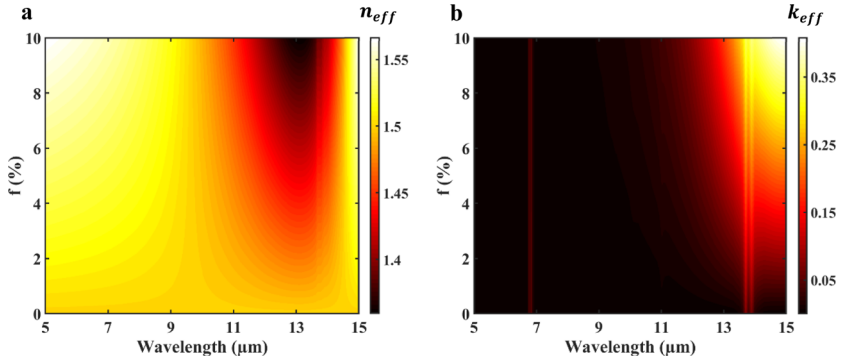

Figure 3. Real n_{eff} (a) and imaginary k_{eff} (b) parts of the refractive index ($N_{eff} = n_{eff} + ik_{eff}$) of a PE membrane as a function of the volume fraction f of TiO_2 particles in the MIR range. The calculations were done using EMT theory.

using Mie theory for a spherical particle of diameter d. Figure 2a shows the extinction cross section in the 5−15 μm range for d varying from 0.2 to 8 μm. Figure 2a evidences that the extinction of the incident electromagnetic wave occurs at both short and long wavelengths for, respectively, particle size larger than 2 and 0.3 μm. Nevertheless, Figure 2b shows that the scattering phenomenon is active for particles of diameters larger than 2 μm and mainly at low wavelengths. The absorption cross section is displayed as a function of d in Figure 2c. It indicates that particles with diameters between 1 μm and 3 μm show high absorption in the 13−15 μm wavelength range. Now, the thermoregulation mechanism of our fabric benefits more from the absorption capabilities of the particles than on the scattering properties of TiO_2 particles. Therefore, the diameter of the particles d should be smaller than 2 μm to obtain minimal diffusion with high absorption.

To better evidence the behaviors of particles with d smaller and larger than 2 μm, we plotted in Figure 2d,e the normalized cross sections Σ_e (black line), Σ_s (blue line), and Σ_a (red line), for d = 1 μm and d = 3 μm, respectively. A particle with d = 1 μm (Figure 2d) shows almost no scattering effect while exhibiting a high absorption for wavelengths larger than 13 μm. However, a particle with d = 3 μm (Figure 2e) strongly scatters at short wavelengths but also at long wavelengths to a lesser

https://doi.org/10.1021/acsomega.5c10457
ACS Omega 2026, 11, 9826−9835

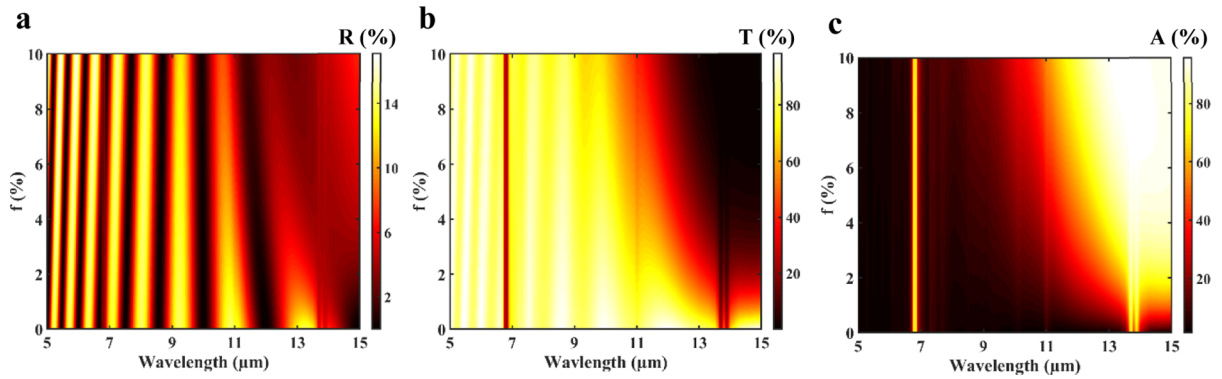

Figure 4. Reflection (a), transmission (b), and absorption (c) coefficients for a PE membrane as a function of volume fraction f of TiO_2 particles in the MIR range. The calculations were done for a normal incidence by using the matrix transfer method. The membrane thickness was chosen equal to e_p = 20 μm.

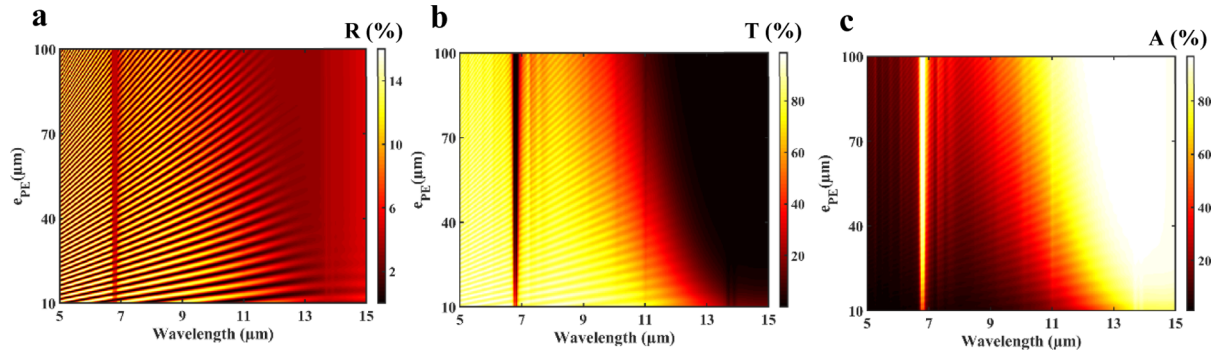

Figure 5. Reflection (a), transmission (b), and absorption (c) coefficients of a PE membrane containing f = 5% of TiO_2 particles as a function of thickness e_p in the MIR range. The calculations were done for a normal incidence using the TMM method.

extent. In the meantime, such a particle is also absorbed in the 13−15 μm wavelength range.

2.2.2. Particles Fraction Effect. After studying the influence of the particle's diameter, we need to assess the impact of the volume fraction f of these spherical particles on the MIR wavelength range. Considering that the particles exhibit low scattering (with diameters below 2 μm), the EMT has been used (Supporting Information) to calculate the effective refractive index N_{eff} as a function of f in the 5−15 μm wavelength range. Figure 3 shows the complex refractive index $N_{eff} = n_{eff} + ik_{eff}$ calculated for f varying from 0% to 10%. In the 13−15 μm range, one can see that the volume fraction f of particles has a strong impact on both the real (n_{eff}, Figure 3a) and imaginary (k_{eff}, Figure 3b) parts of the refractive index of a PE membrane. Comparing a membrane without particles (f = 0%) with one containing particles, one can see that n_{eff} decreases (Figure 3a) while k_{eff} increases (Figure 3b) in the 13−15 μm wavelength range. This behavior is directly related to the contrast between the real and imaginary parts of the two materials: n_{PE} versus n_{TiO_2} and k_{PE} versus k_{TiO_2}, respectively. Actually, at high wavelengths, n_{TiO_2} is smaller than n_{PE}, while the imaginary part k_{TiO_2} is larger than k_{PE}. This evolution of n_{eff} and k_{eff} as a function of f is hence explained by the increased number of TiO_2 particles within the PE matrix.

Using the TMM, both reflection (R) and transmission (T) coefficients have been calculated for a 20 μm-thick membrane containing a volume fraction f of particles. The absorption (A) coefficient was then deduced from the following relationship: $A = 1 - (R + T)$. All three elements are presented in Figure 4a−c, which shows that the volume fraction of particles affects the optical coefficients mainly within the 13−15 μm wavelength range. Actually, increasing f leads to a decrease in R and T, while the absorption coefficient A increases significantly. This change in the three optical coefficients can be explained by the impact of particles on the refractive index, as demonstrated earlier in Figure 3. More specifically, the decrease in n_{eff} leads to a reduction in the refractive index contrast between the polymer layer and the air. Consequently, the reflective part of electromagnetic wave decreases. In parallel, the increase of A is due to the increase of the imaginary part k_{eff}. The effect of the particles on coefficient A leads to a drastic reduction of T. Moreover, a small fraction of particles is useful for other properties, such as the flexibility of the membrane. Thus, a volume fraction of TiO_2 particles lower than f = 5% enables the particle effect to be fully exploited without degrading the flexibility of the PE membrane.

2.2.3. Membrane Thickness Effect. The thickness of the membrane e_p is an important parameter as it can also impact the fabric's MIR optical properties. As previously reported, the effect of the membrane thickness on the three optical coefficients has been studied. The reflection (R, Figure 5a), transmission (T, Figure 5b), and absorption (A, Figure 5c) coefficients were calculated in the MIR wavelength range for a membrane of thickness e_p, varied from 10 to 100 μm. In accordance with our previous findings, the simulated membrane also contained a volume fraction of TiO_2 particles set at f = 5%. Figure 5a clearly shows that increasing e_p has a small impact on the amplitude of R. However, new Fabry−Perot oscillations appear as e_p increases. Figure 5b shows that

https://doi.org/10.1021/acsomega.5c10457
ACS Omega 2026, 11, 9826−9835

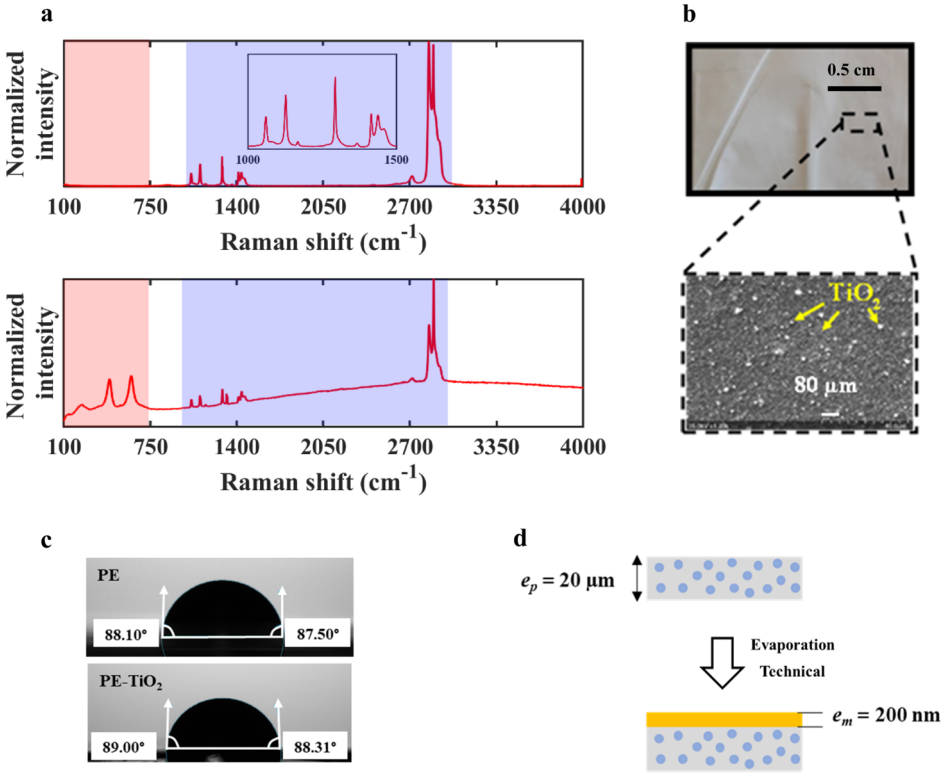

Figure 6. Morphology and fabrication of the VOIMF. (a) Raman spectrum of PE without (top) and with 5 vol % TiO_2 particles (bottom). The blue and red areas outline the signatures of PE and TiO_2, respectively. (b) Snapshot (top) and SEM image (bottom) of the doped PE membrane showing the random distribution of particles inside the polymer matrix. (c) Contact angle of PE (top) and PE-TiO_2 (bottom) showing the incomplete wetting of the two surfaces. (d) 2D schematic representation of the fabrication process of VOIMF.

coefficient T is drastically reduced within a narrow wavelength window, close to 7 μm, due to the simultaneous amplification of the PE's intrinsic absorption peak (Figure 5c). In addition, at high wavelengths, the zero T domain enlarges, going from the [13−15] to [10−15] μm wavelength range with e_p (Figure 5b). The increase in A in the same region (Figure 5c) can be explained by the increase in the interaction between radiation and matter. A composite membrane thickness of e_p = 20 μm makes it possible to obtain high absorption (emissivity) without compromising the fabric's mechanical flexibility.

In conclusion of this theoretical investigation, a PE membrane with a thickness of e_p = 20 μm, containing f = 5% by volume of TiO_2 particles having a diameter d < 2 μm meets the expected optical properties. It can be combined with a metal layer (a thickness of 200 nm of Au has been chosen) to ensure total reflection from one of the two faces.

3. EXPERIMENTAL SECTION

3.1. Morphology and Fabrication

To realize the fabric, we start from the chemical and morphological characterization of a commercial 20 μm-thick doped PE membrane. The doped membrane was fully characterized to better define and demonstrate its properties. The information given below clearly identifies its properties. First, we performed micro-Raman spectroscopy (see the Methods section for details) on multiple random positions of the doped membrane to identify the composite materials of the polymer matrix. Figure 6a shows the Raman spectrum of a PE membrane free of particles, which was taken as reference (top), and that of a PE membrane containing 5% of TiO_2 particles (bottom). The shape of the Raman signatures in the 1000−1500 cm^{-1} range demonstrates that the PE is of the high density polyethylene (HDPE)[44] type. The Raman signatures of HDPE at 1070 and 1135 cm^{-1} are assigned to C−C stretching modes and that at 1300 cm^{-1} to the $-CH_2-$ twisting mode.[44−46] The feature centered at around 1445 cm^{-1} corresponds to the Raman signatures of the $-CH_2-$ bending modes. In addition, the HDPE membrane shows two strong peaks at 2845 cm^{-1} and 2883 cm^{-1} due to the asymmetric and symmetric stretching modes of CH_2, respectively.[44−46] In contrast to the reference, the Raman spectrum corresponding to the HDPE membrane enriched with 5% of TiO_2 particles (Figure 6a, bottom) exhibits new peaks in the 100−750 cm^{-1} spectral range. These new peaks are assigned to the rutile phase of TiO_2 particles.[47] Raman active modes of B_{1g}, E_g, and A_{1g} symmetries appear in the spectrum at 143, 445, and 610 cm^{-1}, respectively. The band at 242 cm^{-1} originates from two-phonon Raman scattering.[48]

The PE membrane contains 20 wt % TiO_2 corresponding to 5 vol %, considering the density ratio of 1 to 5 between PE and TiO_2. Figure 6b shows a representative optical snapshot (top) and scanning electron microscopy (SEM) (bottom) images of the morphology of the PE membrane doped with TiO_2 particles. The dielectric particles (in white on the SEM image) are randomly and uniformly dispersed in the polymer matrix. The SEM image qualitatively highlights a size dispersion of the TiO_2 particles in the micrometer range.

We also characterized the wetting properties of the fabric by measuring the water contact angle of both the reference surface (PE with no particles) and PE with TiO_2 particles (see the Methods section). Both surfaces show the same static contact angles (resulting in a nearly hydrophobic surface), demonstrating that there is no change in surface properties with or without TiO_2 (see Figure 6c). Beyond the exploring nature of our work on the optical and thermal properties of the model textile sample, it should be noted that this property could have an impact to extend the life of textiles by protecting them from moisture and mold, making garments more functional and durable.

Once the PE-5 vol %TiO_2 membrane had been successfully characterized, we proceeded to manufacture the bilayered membrane. To do so, we metallized (evaporation method) the PE-5 vol %TiO_2

https://doi.org/10.1021/acsomega.5c10457
ACS Omega 2026, 11, 9826−9835

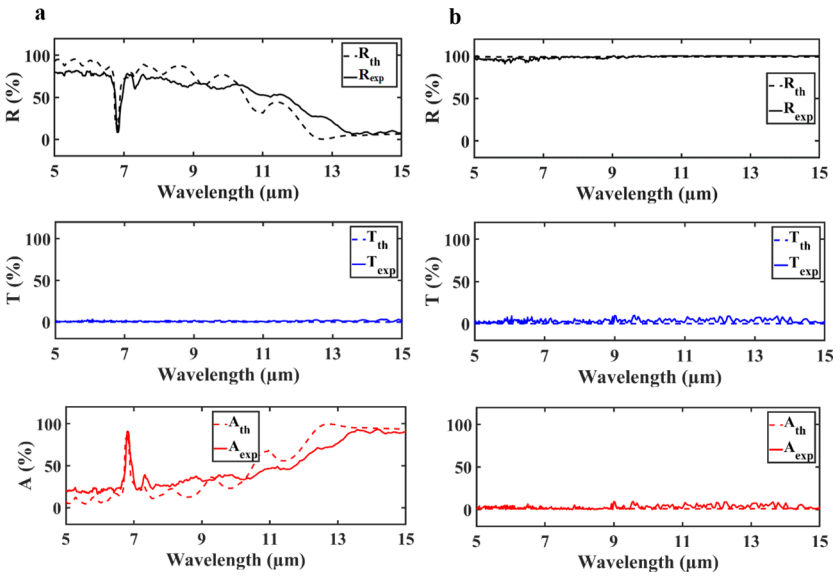

Figure 7. Simulated (dashed line) and measured (solid line) MIR properties of the VOIMF. *R* (black line), *T* (blue line), and *A* (red line) coefficients for an incident wave facing either the doped polymer layer (a) or the metallic one (b). The numerical simulations were done using FEM and the measurements were performed with an FTIR spectrometer.

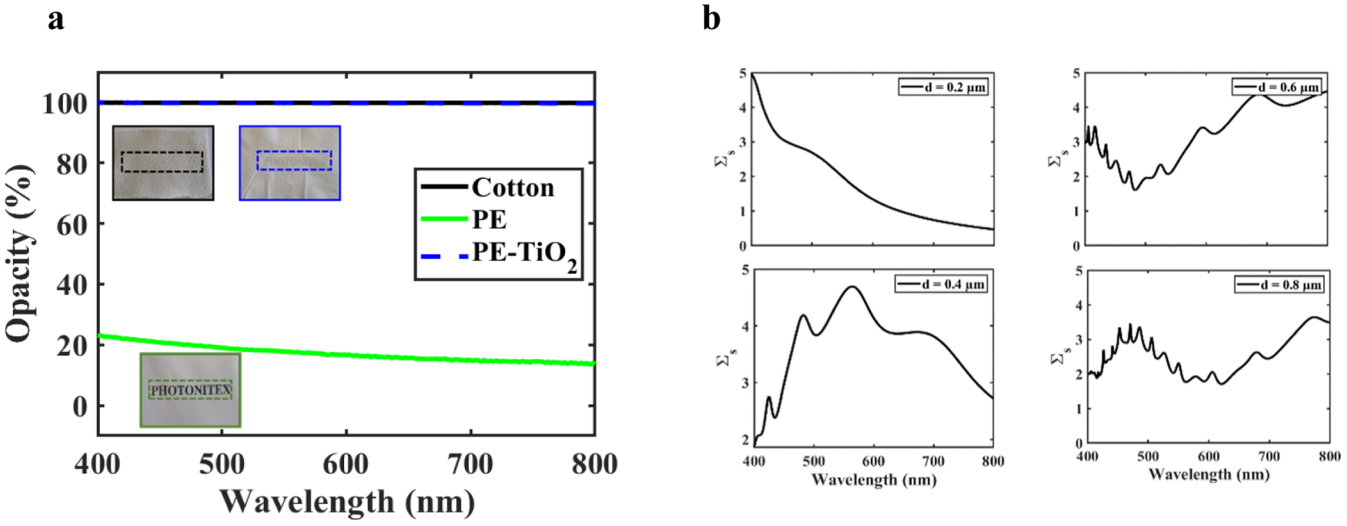

Figure 8. Optical properties of PE-5 vol %TiO_2 in the visible range. (a) Measured opacity of cotton (black), PE (green), PE-TiO_2 (blue). (b) Normalized cross section of scattering Σ_s as a function of particle diameter *d* in the VIS range of 400−800 nm for $d = 0.2$ μm, $d = 0.4$ μm, $d = 0.6$ μm, and $d = 0.8$ μm. The calculation was done for a single TiO_2 particle in the PE medium using Mie theory.

membrane with an ultrathin Au layer of thickness e_{Au} = 200 nm (see Figure 6d). For large-scale manufacturing, methods such as roll bonding and roll-to-roll processing can be used.[49,50]

3.2. MIR Properties

The MIR properties of the two configurations of the VOIMF were studied theoretically and experimentally. Using the FEM (see the Methods section for details), we have calculated the optical coefficients of the VOIMF in the 5−15 μm range. The measurement has been done using an Fourier transform infrared spectroscopy (FTIR) spectrometer with a gold integrated sphere (see the Methods section). Figure 7 shows the simulated (dashed line) and measured (solid line) *R* (black line), *T* (blue line), and *A* (red line) coefficients when the incident wave faces either the doped polymer layer (Figure 7a) or the metallized one (Figure 7b). The fabric shows an asymmetrical behavior in the MIR. In both cases, the transmission is zero due to the metallic layer. Nevertheless, in the first configuration (Figure 7a), one can see a high reflection in the [5−9] μm range and high absorption in the [10−15] μm range due to the TiO_2 particles (see Section 3). The second configuration (Figure 7b), with the incident wave facing the metalized side, leads to a total reflection in the MIR range. The thermal behavior of these two modes will be considered in the last section.

3.3. Visible Properties

The visible (VIS) properties of the proposed VOIMF in both configurations were addressed by measuring the fabric's visible transmission spectra (refer to the Methods section for details), from which the opacity is deduced using the following relationship: VIS opacity = 100% − Transmission. Figure 8a shows the measured opacities of cotton (black), PE (green), and PE-TiO_2 (blue). Looking at Figure 8a, one can see that the regular PE shows a relative transparency, with 20% opacity, while the PE-TiO_2 shows high visible opacity close to 100%, similar to that of cotton textile. The snapshots presented in Figure 8a were taken with a camera and show the different membranes covering the name of our European project 'PHOTONITEX'. To understand the VIS property of PE-TiO_2, we calculated the scattering properties of a single TiO_2 particle

https://doi.org/10.1021/acsomega.5c10457
ACS Omega 2026, 11, 9826−9835

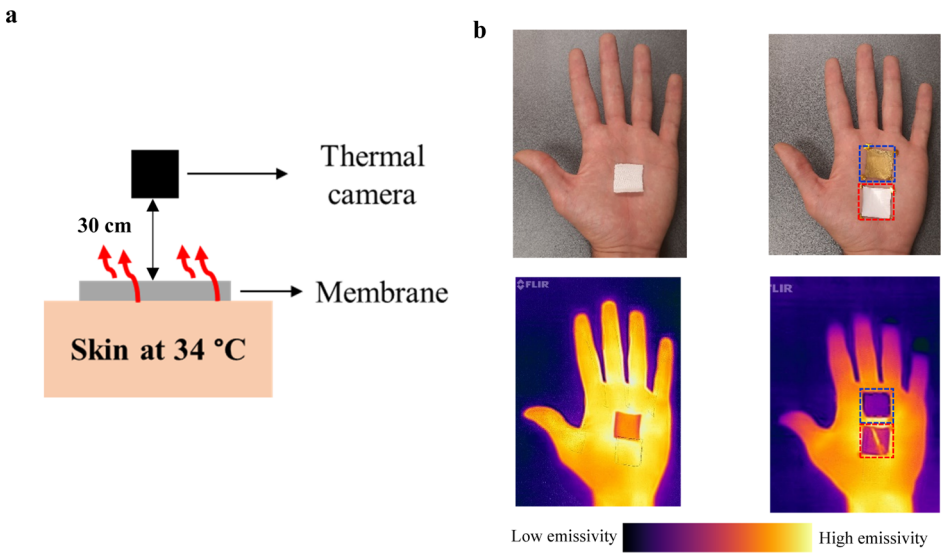

Figure 9. Infrared camera visualization of the transmitted and emitted thermal radiation by the membranes. (a) Schematic of the measurement process. (b) Optical (top) and thermal (bottom) images of the hand's covered by cotton (left) and the fabric (right) in Mode 1 (red frame) and Mode 2 (blue frame). The thermal image is taken at an ambient temperature of 25 °C and at 30 cm from the hand.

embedded in a PE medium in the [400−800] nm range. Figure 8b represents the normalized cross section of scattering ($\Sigma_s = \frac{4\sigma_s}{\pi d^2}$) for diameters d = 0.2 μm, d = 0.4 μm, d = 0.6 μm, and d = 0.8 μm. The combined effect of the different diameters results in strong scattering of all wavelengths in the visible (VIS) range, leading to the white appearance and opacity of the doped PE membrane. Therefore, the VOIMF appears white and opaque to the human eye in Mode 1 and exhibits a gold color in Mode 2. Moreover, from a visual point of view, if we consider the use of this type of sample as is, in order to avoid the metallic sheen of the gold layer in operating Mode 2, an additional PE layer doped with oxide zinc (ZnO) particles may be added. Because both PE and ZnO have low absorption in the MIR and ZnO provides strong scattering in the visible range, this layer will give the membrane a white appearance.[12]

3.4. Outgoing Thermal Radiation Characterization

In this section, we demonstrate the ability of VOIMF to control the infrared emissivity toward the environment. This aspect is directly related to the numerous studies that have previously demonstrated that the emissivity of a textile's outer surface plays a decisive role in controlling thermoregulation performance.[1,4,26] Using a thermal camera, we qualitatively recorded the external emissivity of the VOIMF in both operating modes and compared it with that of conventional cotton. We placed the fabric on the palm of a hand at a temperature of 34 °C and then characterized its IR emissivity using a thermal camera in a room at temperature 25 °C (see Figure 9a). The camera was placed approximately 30 cm from the palm of the hand. Figure 9b shows the optical (top) and thermal (bottom) images of the two samples deposited on the hand, namely, the cotton (left images) and the PE/TiO_2−Au in two operating modes (right image, red and blue frame). It can be seen that the cotton has a warm color (orange) compared to both sides of the fabric, indicating a high emissivity corresponding to heat losses by radiation. Depending on which side is facing the thermal camera, the fabric behaves in two different ways. When the fabric is operating in Mode 1 (red frame), the fabric appears in warm color, which means that the fabric is emitting a high level of thermal radiation. When the fabric is switched to Mode 2 (blue frame), the fabric color is then perceived as blue by the thermal camera, which means that the fabric is emitting a low level of thermal radiation. It means that in the first case, the thermal energy is mainly restituted to the environment, while in the second one, the thermal energy is mainly restituted to the body's microclimate. Compared with conventional textiles that operate in a single high-emissivity mode, these results qualitatively show the fabric's ability to control radiative emission toward the environment.

4. THERMAL ANALYSIS

To further demonstrate the thermoregulation performance of VOIMF, we quantitatively compared the added value of our fabric with that of a conventional textile. We chose a cotton textile with a thickness of 360 μm (18 × e_p). The optical coefficients, measured by FTIR, are presented in Figure S2 (Supporting Information). Using an analytical thermal model, we calculated the ambient set-point temperature necessary to maintain the skin temperature at 34 °C (i.e., the room temperature required for thermal comfort when wearing different textiles). The analytical model is detailed in the Supporting Information (see Supporting Note 3). The calculation was performed for both VOIMF configurations and compared to a layer of cotton. As shown in Figure 10a, the

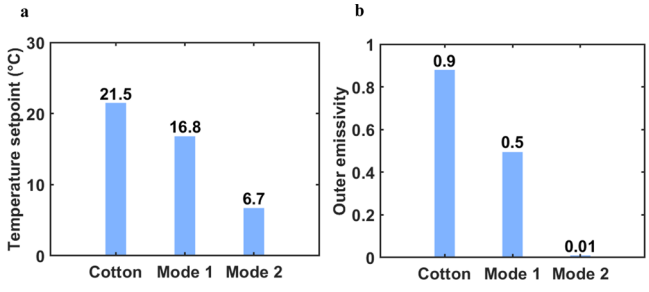

Figure 10. Comparison of conventional cotton and VOIMF modes in terms of their comfort temperature set points (i.e., room temperature required for thermal comfort when wearing different textiles) (a) and their outer emissivity (b).

conventional cotton textile maintains thermal comfort only at a room temperature of 21.5 °C. However, our fabric shows dual behavior. When the VOIMF is set to Mode 1, the human body remains thermally comfortable at a room temperature of 16.8 °C. When the VOIMF is reversed to Mode 2, the comfort set point decreases to 6.7 °C. This behavior is directly related to the emissivity of the membrane, which can be estimated from

https://doi.org/10.1021/acsomega.5c10457
ACS Omega 2026, 11, 9826−9835

the outer side of the textile (Figure 10b). For the cotton layer, we get a single value of 0.9 which is efficient for a room temperature of 21.5 °C. For lower temperature the VOIMF demonstrates its efficiency by limiting the radiative emission to the environment to 0.5 then 0.01. However, the asymmetric emissivity of the VOIMF allows the switching between higher and lower heat losses. Compared to previous dual-mode textiles and Janus structures,[23−27] the VOIMF exhibits a wider thermal comfort zone, extending to lower temperatures. Overall, these papers present heating properties ranging from 8.3 to 33 °C. However, our work differs from other studies in that it has a lower minimum temperature. Previously, our work had resulted in a range from 7.1 to 16.3 °C (ref 26), whereas in this article, we have managed to achieve a range from 6.7 to 16.8 °C, which is not only wider in scope but also lower in temperature than what has been published to date to our best knowledge. Therefore, a textile based on a VOIMF can be an effective solution to replace a conventional textile for a low-temperature environment.

5. CONCLUSION

In conclusion, we have developed a fabric with a high heating performance for thermoregulation in low-temperature indoor environments. By modulating its outer emissivity in the MIR range, the fabric maintains thermal comfort of the human body in the ambient temperature range of 6.7−16.8 °C. The wide thermal comfort zone (∼10 °C) achieved by the fabric can considerably reduce the energy consumption in buildings. Moreover, the fabric remains opaque to human eyes due to the high TiO_2 particle scattering property of visible wavelengths. The results obtained from a test sample are the first step toward optimizing the textiles worn. By considering possible modifications to the materials used (membranes made from other types of porous polymers, for example, to improve the breathability of the textile, different metals to be taken into account depending on their cost price, other particles to modify both the optical properties in the infrared and visible spectrum, etc.), we have also attempted to broaden the application prospects of the VOIMF.

An additional advantage of this textile is its ability to maintain thermal comfort at low ambient temperatures with a minimal thickness. This makes it particularly useful for workers in refrigerated warehouses, where temperatures are typically maintained well below 6.7 °C, or for outdoor workers in polar or high-altitude regions exposed to extreme cold conditions, offering a lightweight and comfortable solution for thermal insulation without compromising mobility or wearability.

6. METHODS

6.1. Numerical Simulation

The reflection (R) and transmission (T) coefficients of the VOIMF were calculated using COMSOL Multiphysics software, deducing the absorption by $A = 100\% - (R + T)$. An elementary cell of the VOIMF was considered in air, and a periodic boundary condition was applied to generate all geometries. A source and a detector of the electromagnetic wave were placed before and after the elementary cell. The source generates a plan wave propagating in air and penetrating the design at normal incidence. The efficiency coefficient was calculated by ρ, τ, $\alpha = \frac{\int_5^{15} E_\lambda \chi_\lambda d\lambda}{\int_5^{15} E_\lambda d\lambda}$, where E_λ is the human body emissivity calculated by Planck's law and χ_λ is the R, T, and A coefficients at wavelength λ.

6.2. Raman Spectroscopy

Raman spectra were acquired using a Renishaw inVia Reflex spectrometer coupled to an optical free-space microscope (BXFM Olympus), mounted with a 50X (0.5 N.A.) Olympus LMPlanFl magnification objective. An excitation wavelength of 514.5 nm with a 150 mW nominal power (DPSS laser, Cobolt) was used. Laser power was reduced at the sample to 10% of the nominal power, and the minimum beam spot size was about 1.3 μm. A spectral resolution of ∼ 12 cm^{-1} was obtained when using the 600 grooves/mm diffraction grating, and the Raman backscattered photons are collected on a CCD camera (576 × 400 pixels) cooled by the Peltier effect. The correct position of the peaks was ensured by calibration of the instrument against the signature of a silicon standard at 520 cm^{-1}. Each spectrum corresponds to an accumulation of 3 scans with a total collection time of 90 s in extended mode (100−4000 cm^{-1}).

6.3. Scanning Electron Microscopy

The surface morphology of the membrane was characterized using SEM (Hitachi SEM field emission GU) with an accelerating voltage of 5 kV and an emission current of 10 μA. Before imaging, the membrane was sputtered with a thin layer of chrome.

6.4. Contact Angle

The contact angle of the samples was measured using water as the liquid with Biolin Scientific.

6.5. Metallization

The composite PE membrane was metallized using electron beam physical vapor deposition in an IEMN cleaning room. The speed of deposit was 1 nm s^{-1}.

6.6. Fourier Transform Infrared Spectroscopy

The MIR properties of the samples were characterized by an FTIR Prestige 21 (from Shimadzu) spectrometer with a gold sphere integrating system (from PIKE Technologies). The transmission (T) measurements were performed at normal incidence. For the reflection (R) measurements, the angle of incidence is 12°. The absorption (A) was calculated by $A = 100\% - (R + T)$.

6.7. UV−Vis Spectroscopy

The VIS properties of the samples were characterized by using a Lambda 800 UV/vis Spectrometer from PerkinElmer. The measurements were done in air at a normal incidence.

6.8. Emissivity Characterization

The outer emissivity of the sample was characterized via an infrared camera by using a testo 865. The thermal images were taken in an indoor area at normal humidity.

■ ASSOCIATED CONTENT

Supporting Information

The Supporting Information is available free of charge at https://pubs.acs.org/doi/10.1021/acsomega.5c10457.

Effective medium theory (Note 1), MIR properties of cotton (Note 2), and the analytical thermal model (Note 3) (PDF)

■ AUTHOR INFORMATION

Corresponding Author

Mohamed Boutghatin − *IEMN—Institut d'Electronique de Microélectronique et de Nanotechnologie, Univ. Lille, CNRS, Univ Polytechnique Hauts-de-France, Centrale Lille, UMR 8520, F-59000 Lille, France;* orcid.org/0000-0002-5486-917X; Email: mohamed.boutghatin@univ-lille.fr

https://doi.org/10.1021/acsomega.5c10457
ACS Omega 2026, 11, 9826−9835

Authors

Claire Pirim − *Univ. Lille, CNRS, UMR 8523 − PhLAM—Physique des Lasers Atomes et Molécules, F-59000 Lille, France;* orcid.org/0000-0001-5942-5001

Valérie Gaucher − *INRAE, Centrale Lille, UMET-Unité Matériaux et Transformations, Univ. Lille, CNRS, UMR 8207, F-59000 Lille, France*

Yannick Coffinier − *Univ. Lille, CNRS, Univ Polytechnique Hauts-de-France, UMR 8520, IEMN - Institut d'Electronique de Microélectronique et de Nanotechnologie, F-59000 Lille, France;* orcid.org/0000-0001-7433-2102

Bahram Djafari Rouhani − *Univ. Lille, CNRS, Univ Polytechnique Hauts-de-France, UMR 8520, IEMN - Institut d'Electronique de Microélectronique et de Nanotechnologie, F-59000 Lille, France*

Vincent Thomy − *Univ. Lille, CNRS, Univ Polytechnique Hauts-de-France, UMR 8520, IEMN - Institut d'Electronique de Microélectronique et de Nanotechnologie, F-59000 Lille, France*

Yan Pennec − *Univ. Lille, CNRS, Univ Polytechnique Hauts-de-France, UMR 8520, IEMN - Institut d'Electronique de Microélectronique et de Nanotechnologie, F-59000 Lille, France*

Michele Carette − *Univ. Lille, CNRS, Univ Polytechnique Hauts-de-France, UMR 8520, IEMN - Institut d'Electronique de Microélectronique et de Nanotechnologie, F-59000 Lille, France*

Complete contact information is available at: https://pubs.acs.org/10.1021/acsomega.5c10457

Notes

The photos in Figure 9 were taken by Mohamed Boutghatin. The authors declare no competing financial interest.

■ ACKNOWLEDGMENTS

This work was partially supported by the French Renatech network and partially undertaken with the support of IEMN fabrication (CMNF). The authors acknowledge the French National Agency (ANR) for its financial support (POCOMA Project-ANR-21-CE09-0040) and the Interreg program 1340 (Project ANR-17-CE08-0032).

■ REFERENCES

(1) Cai, L.; Song, A. Y.; Wu, P.; Hsu, P. C.; Peng, Y.; Chen, J.; Liu, C.; Catrysse, P. B.; Liu, Y.; Yang, A.; et al. Warming up human body by nanoporous metallized polyethylene textile. *Nat. Commun.* **2017**, *8*, 496.

(2) Hardy, J. D.; DuBois, E. F. Regulation of Heat Loss from the Human Body. *Proc. Natl. Acad. Sci. U. S. A.* **1937**, *23*, 624−631.

(3) Ullah, H. M. K.; et al. A review of noteworthy/major innovations in wearable clothing for thermal and moisture management from material to fabric structure. *Text. Res. J.* **2022**, *92*, 3351−3386.

(4) Lan, X.; et al. Designing Heat Transfer Pathways for Advanced Thermoregulatory Textiles. *Mater. Today Phys.* **2021**, *17*, 100342.

(5) Hu, R.; Liu, Y.; Shin, S.; Huang, S.; Ren, X.; Shu, W.; Cheng, J.; Tao, G.; Xu, W.; Chen, R.; et al. Emerging Materials and Strategies for Personal Thermal Management. *Adv. Energy Mater.* **2020**, *10*, 1903921.

(6) Boutghatin, M.; et al. Impact of SiO2 Particles in Polyethylene Textile Membrane for Indoor Personal Heating. *Nanomaterials* **2020**, *10*, 1968.

(7) Assaf, S.; Boutghatin, M.; Pennec, Y.; Thomy, V.; Korovin, A.; Treizebre, A.; Carette, M.; Akjouj, A.; Djafari-Rouhani, B. Polymer photonic crystal membrane for thermo-regulating textile. *Sci. Rep.* **2020**, *10*, 9855.

(8) Boutghatin, M.; et al. Polymer-Based Microstructured Photonic Membrane for Passive Heating Textiles. *ACS Omega* **2025**, *10*, 40922−40929.

(9) Liu, Q.; et al. Thermal, Waterproof, Breathable, and Antibacterial Cloth with a Nanoporous Structure. *ACS Appl. Mater. Interfaces* **2018**, *10*, 2026−2032.

(10) Hsu, P.-C.; et al. Radiative human body cooling by nanoporous polyethylene textile. *Science* **2016**, *353*, 1019−1023.

(11) Cai, L.; et al. Temperature Regulation in Colored Infrared-Transparent Polyethylene Textiles. *Joule* **2019**, *3*, 1478−1486.

(12) Cai, L.; Song, A. Y.; Li, W.; Hsu, P. C.; Lin, D.; Catrysse, P. B.; Liu, Y.; Peng, Y.; Chen, J.; Wang, H.; et al. Spectrally Selective Nanocomposite Textile for Outdoor Personal Cooling. *Adv. Mater.* **2018**, *30*, No. e1802152.

(13) Hsu, P.-C.; et al. Personal Thermal Management by Metallic Nanowire-Coated Textile. *Nano Lett.* **2015**, *15*, 365−371.

(14) Peng, Y.; et al. Nanoporous polyethylene microfibres for large-scale radiative cooling fabric. *Nat. Sustain.* **2018**, *1*, 105−112.

(15) Wei, W.; et al. An Al2O3-cellulose acetate-coated textile for human body cooling. *Sol. Energy Mater. Sol. Cells* **2020**, *211*, 110525.

(16) Yue, X.; et al. Ag nanoparticles coated cellulose membrane with high infrared reflection, breathability and antibacterial property for human thermal insulation. *J. Colloid Interface Sci.* **2019**, *535*, 363−370.

(17) Woo, H. K.; Zhou, K.; Kim, S. K.; Manjarrez, A.; Hoque, M. J.; Seong, T. Y.; Cai, L. Visibly Transparent and Infrared Reflective Coatings for Personal Thermal Management and Thermal Camouflage. *Adv. Funct. Mater.* **2022**, *32*, 2201432.

(18) Chai, J.; et al. Thermoregulatory clothing with temperature-adaptive multimodal body heat regulation. *Cell Rep. Phys. Sci.* **2022**, *3*, 100958.

(19) Zeng, S. Hierarchical-morphology metafabric for scalable passive daytime radiative cooling, *Science*, **2021**; Vol. *373*, 692696.

(20) Boutghatin, M.; et al. Dynamic thermoregulatory photonic crystal fabric for personal thermal management. In *2021 IEEE Sensors*; IEEE: Sydney, Australia, 2021; pp 1−4.

(21) Higueros, G.; Li, Q.; Hsu, P.-C. Perspective on the Next Ten Years of Wearable Passive Radiative Thermoregulation. *ACS Mater. Lett.* **2025**, *7*, 1879−1886.

(22) Yao, W.; Zhu, G.; Yan, Z.; Tong, W.; Fan, D. Revolutionizing personal thermal management technologies with advanced materials and strategies. *Appl. Mater. Today* **2025**, *44*, 102719.

(23) Wang, X.; et al. A Passive Sweat-Responsive Thermoregulatory Textile with the Largest Thermal Comfort Zone. *ACS Nano* **2025**, *19*, 19977−19988.

(24) Yue, X.; et al. Multifunctional Janus fibrous hybrid membranes with sandwich structure for on-demand personal thermal management. *Nano Energy* **2019**, *63*, 103808.

(25) Hsu, P.-C.; Liu, C.; Song, A. Y.; Zhang, Z.; Peng, Y.; Xie, J.; Liu, K.; Wu, C. L.; Catrysse, P. B.; Cai, L.; et al. A dual-mode textile for human body radiative heating and cooling. *Sci. Adv.* **2017**, *3*, No. e1700895.

(26) Boutghatin, M.; Pennec, Y.; Djafari-Rouhani, B.; Akjouj, A.; Gaucher, V.; Gidik, H.; Assaf, S.; Carette, M.; Thomy, V. Asymmetric Design for a High-Performance Indoor Radiative Heating Fabric. *Adv. Mater. Technol.* **2022**, *7*, 2101738.

(27) Pian, S.; et al. Scalable colored Janus fabric scheme for dynamic thermal management. *iScience* **2024**, *27*, 110948.

(28) Leung, E. M.; Colorado Escobar, M.; Stiubianu, G. T.; Jim, S. R.; Vyatskikh, A. L.; Feng, Z.; Garner, N.; Patel, P.; Naughton, K. L.; Follador, M.; et al. A dynamic thermoregulatory material inspired by squid skin. *Nat. Commun.* **2019**, *10*, 1947.

(29) Zhang, X. A.; et al. Dynamic gating of infrared radiation in a textile. *Science* **2019**, *363*, 619−623.

(30) Abebe, M. G.; et al. Dynamic Thermal-Regulating Textiles with Metallic Fibers Based on a Switchable Transmittance. *Phys. Rev. Applied* **2020**, *14*, 044030.

(31) Xu, Z.; et al. Nonvolatile Optically Reconfigurable Radiative Metasurface with Visible Tunability for Anticounterfeiting. *Nano Lett.* **2021**, *21*, 5269−5276.
(32) Huang, Y.; Zhu, H.; Zhou, Y.; Dai, C.; Zhu, R.; Ghosh, P.; Qiu, M.; Li, Q. Adaptive visible-infrared camouflage with wide-range radiation control for extreme ambient temperatures. *PhotoniX* **2025**, *6*, 25.
(33) *Handbook of Optical Constants of Solids II*; Palik, E. D., Ed.; Academic Press: Boston, 1991.
(34) Boriskina, S. V. An ode to polyethylene. *MRS Energy Sustain.* **2019**, *6*, 14.
(35) Gulmine, J. V.; Janissek, P. R.; Heise, H. M.; Akcelrud, L. Polyethylene characterization by FTIR. *Polym. Test.* **2002**, *21*, 557−563.
(36) Handbook of Polyethylene Structures Properties, and Applications (Plastics Engineering) by Andrew Peacock; pdf.
(37) Kischkat, J.; et al. Mid-infrared optical properties of thin films of aluminum oxide, titanium dioxide, silicon dioxide, aluminum nitride, and silicon nitride. *Appl. Opt.* **2012**, *51*, 6789.
(38) Vargas, W. E. Optimization of the diffuse reflectance of pigmented coatings taking into account multiple scattering. *J. Appl. Phys.* **2000**, *88*, 4079.
(39) Hu, S.; Li, F.; Fan, Z. Preparation of SiO_2-Coated TiO_2 Composite Materials with Enhanced Photocatalytic Activity Under UV Light. *Bull. Korean Chem. Soc.* **2012**, *33*, 1895−1899.
(40) Tania, I. S.; Ali, M. Utilization of titanium dioxide (TiO2) nanoparticles to improve functionality and mechanical performances of cotton fabric. *Heliyon* **2024**, *10*, No. e37899.
(41) Katsidis, C. C.; Siapkas, D. I. General transfer-matrix method for optical multilayer systems with coherent, partially coherent, and incoherent interference. *Appl. Opt.* **2002**, *41* (19), 3978−3987.
(42) Bohren, C. F.; Huffman, D. R. *Absorption and Scattering of Light by Small Particles*; Wiley: New York, 1983.
(43) Garahan, A.; Pilon, L.; Yin, J.; Saxena, I. Effective optical properties of absorbing nanoporous and nanocomposite thin films. *J. Appl. Phys.* **2007**, *101*, 014320.
(44) Allen, V.; Kalivas, J. H.; Rodriguez, R. G. Post-Consumer Plastic Identification Using Raman Spectroscopy. *Appl. Spectrosc.* **1999**, *53*, 672−681.
(45) Bentley, P. A.; Hendra, P. J. Polarised FT Raman studies of an ultra-high modulus polyethylene rod. *Spectrochim. Acta, Part A* **1995**, *51*, 2125−2131.
(46) Silva, D. J. d.; Wiebeck, H. Predicting LDPE/HDPE blend composition by CARS-PLS regression and confocal Raman spectroscopy. *Polímeros - Ciência Tecnol.* **2019**, *29*, No. e2019010.
(47) Hardcastle, F. D. Raman Spectroscopy of Titania (TiO_2) Nanotubular Water-Splitting Catalysts. *Ark. Acad. Sci.* **2011**, *65*..
(48) Tuschel, D. Raman Spectroscopy and Polymorphism. *Spectroscopy* **2019**, *34*, 10−21.
(49) Park, J.; Shin, K.; Lee, C. Roll-to-Roll Coating Technology and Its Applications: A Review. *Int. J. Precis. Eng. Manuf.* **2016**, *17*, 537−550.
(50) Mousa, S.; Scheirer, N.; Kim, G.-Y. Roll-bonding of metal-polymer-metal sandwich composites reinforced by glass whiskers at the interface. *J. Mater. Process. Technol* **2018**, *255*, 463−469.

https://doi.org/10.1021/acsomega.5c10457
ACS Omega 2026, 11, 9826−9835